JOURNAL OF NANO- AND ELECTRONIC PHYSICS *ЖУРНАЛ НАНО- ТА ЕЛЕКТРОННОЇ ФІЗИКИ*
Vol. **7** No 2, 02039(6pp) (2015) Том **7** № 2, 02039(6cc) (2015)

Slab Waveguide Sensor with Left-handed Material Core Layer for Detection an Adlayer Thickness and Index

Hani M. Kullab, Ibrahim M. Qadoura, Sofyan A. Taya

Physics Department, Islamic University of Gaza, P.O. Box 108, Gaza, Palestinian Authority

(Received 01 November 2014; published online 10 June 2015)

A four-layer slab waveguide structure with a lossy left-handed material (LHM) core layer is investigated as a surface sensor for detection any change in an adlayer thickness and refractive index. The sensitivities of the effective refractive index to any change in the refractive index/thickness of the adlayer are derived and studied with the parameters of the LHM. It is found that a slight change in the real parts of the permittivity and permeability of the LHM can significantly improve the sensitivity of the proposed sensor.

Keywords: Left-handed materials, Waveguides, Surface sensing.

PACS numbers: 42.65.Wi, 42.65.Tg, 42.25.Bs

1. INTRODUCTION

Optical planar waveguide sensors are widely recognized as valuable devices for investigating surface interactions, biosensing, quantifying protein adsorption, affinity-based recognition and attachment of bacteria and living cells [1-15]. Optical slab waveguides have proven to be highly sensitive. In surface sensing mechanism, the waveguide configuration is similar to that of the conventional three-layer waveguide with additional layer sandwiched between core and cladding layers called adlayer. In biosensing applications, the adlayer medium contains the biological molecules, proteins, bacteria or living cells to be detected. Accordingly, adsorption of these substances shifts the refractive index at the film-clad interface which can be detected by observing change in reflectivity or effective index of refraction of the guided mode.

Electromagnetic wave propagation in materials with simultaneous negative dielectric permittivity ε and magnetic permeability μ has been first investigated by Veselago [16] who has shown that in such media, Poynting vector is anti-parallel to the direction of energy flow. Such media is referred to as left-handed materials (LHMs). Park et al. [17] introduced the frequency-dependent complex permittivity and permeability of LHMs in the form

$$\varepsilon(\omega) = 1 - \frac{\omega_p^2}{\omega^2 + i\gamma\omega}, \quad (1)$$

$$\mu(\omega) = 1 - \frac{F\omega^2}{\omega^2 - \omega_o^2 + i\gamma\omega}, \quad (2)$$

where ω_p is the plasma frequency, ω_o is the resonance frequency, γ is the electron scattering rate, and F is the fractional area of the unit cell occupied by the split ring. LHMs have been widely investigated [18-31] for possible applications in cloaking devices, perfect lens, and integrated optical devices.

In this work, a four-layer slab waveguide structure with a lossy LHM core film is considered for surface sensing applications. The dispersion relation and the sensitivity of the effective refractive index to variations in the refractive index / thickness of the adlayer are investigated. The effects of the LHM permittivity and permeability on the sensitivity of the proposed sensor are studied. The behavior of the sensitivity curves with the adlayer index is also investigated.

2. THEORY

We consider four-layer slab waveguide structure as shown in Fig. 1. It consists of a LHM guiding film with negative permittivity ε_2, negative permeability μ_2 and thickness d_1. The relatively thick substrate and cladding have parameter (ε_1, μ_1) and (ε_4, μ_4) respectively. An adlayer of permittivity ε_3, permeability μ_3 and thickness d_2 is assumed to be located between the cladding and the guiding film. We consider s-polarized waves (TE) in which the electric field E is polarized along the y-axis.

2.1 Dispersion Relation

Waves are assumed to propagate along x-axis such that $E_y \propto e^{i\beta x}$, where β is the propagating constant along x. Time harmonic fields have the form $E_y(x,z,t) = E_y(z)e^{i(\beta x - \omega t)}$, with ω is the angular frequency. Due to the uniformity of the waveguide structure, the fields are uniform in y direction and Helmholtz equation for the electric field reduces to an ordinary linear second order differential equation as

$$\frac{d^2E_y(z)}{dz^2} + (k_o^2\varepsilon_i\mu_i - \beta^2)E_y(z) = 0, \; i = 1, 2, 3, 4. \quad (3)$$

The effective refractive index for the guided mode N is given by $\beta = k_o N$, where $k_o = \omega\sqrt{\varepsilon_o\mu_o}$. Helmholtz equation becomes

$$\frac{d^2E_y(z)}{dz^2} + k_o^2(\varepsilon_i\mu_i - N^2)E_y(z) = 0, \; i = 1, 2, 3, 4 \quad (4)$$

The waveguide structure under consideration can support a finite number of guided modes and an infinite number of radiation modes. For guided mode solu-

tion, most of the power carried by the wave is confined in the guiding film. Oscillatory solutions are assumed in the guiding film such that $\varepsilon_2\mu_2 - N^2 > 0$ and evanescent tails in all other layers for which $\varepsilon_1\mu_1 - N^2 < 0$, $\varepsilon_3\mu_3 - N^2 < 0$ and $\varepsilon_4\mu_4 - N^2 < 0$.

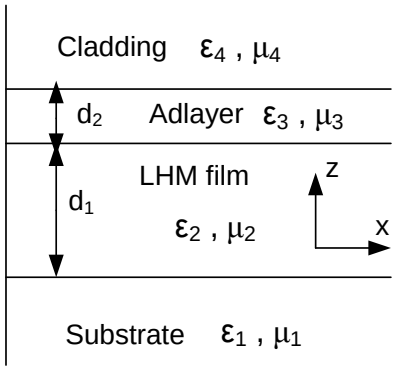

Fig. 1 – Four-Layer planar waveguide structure with a left-handed material core film

The solutions of Helmholtz equation for TE modes in the four layers are given by

$$E_y^{(1)} = A_1 e^{\gamma_s z}, \; z \le 0 \tag{5}$$

$$E_y^{(2)} = A_2 \cos(\gamma_f z) + A_3 \sin(\gamma_f z), \; 0 \le z \le d_1 \tag{6}$$

$$E_y^{(3)} = A_4 e^{\gamma_a (z-d_1)} + A_5 e^{-\gamma_a (z-d_1)}, \; d_1 \le z \le d_2 \tag{7}$$

$$E_y^{(4)} = A_6 e^{-\gamma_c (z-d_1-d_2)}, \; z \ge d_1 + d_2 \tag{8}$$

where $\gamma_s = k_o\sqrt{N^2 - \varepsilon_1\mu_1}$, $\gamma_f = k_o\sqrt{\varepsilon_2\mu_2 - N^2}$, $\gamma_a = k_o\sqrt{N^2 - \varepsilon_3\mu_3}$ and $\gamma_c = k_o\sqrt{N^2 - \varepsilon_4\mu_4}$.

The constants $A_1 - A_6$ represent the amplitudes of the waves in the four layers. Using Eqs. (5)-(8), H_x can be calculated in the different media using $H_x(z) = \frac{i}{\omega\mu(z)}\frac{\partial E_y(z)}{\partial z}$. Matching E_y and H_x at $z = 0$, d_1 and $d_1 + d_2$, we obtain the following dispersion relation

$$\gamma_f d_1 = \tan^{-1}\left(\frac{\gamma_s\mu_2}{\gamma_f\mu_1}\right) + \\ + \tan^{-1}\left(\frac{\gamma_a\mu_2(\gamma_a\mu_4 + \gamma_c) - (\gamma_a\mu_4 - \gamma_c)e^{-2\gamma_a d_2}}{\gamma_f(\gamma_a\mu_4 + \gamma_c) + (\gamma_a\mu_4 - \gamma_c)e^{-2\gamma_a d_2}}\right) + m\pi \tag{9}$$

where $m = 0, 1, 2,\ldots$ is the mode order.

2.2 Power Flow Through Waveguide Layers

In this subsection, the power carried by each layer is derived to fully investigate the four-layer slab waveguide structure under consideration. The guided wave power per unit length a long x-axis is given by

$$P_{total} = \frac{k_o N}{2\omega}\int_{-\infty}^{\infty}\frac{|E_y|^2}{\mu(z)}dz. \tag{10}$$

Using Eqs. (5)-(8) to evaluate the integral given by Eq. (10), we obtain

$$P_s = \frac{k_o N A_1^2}{4\omega\mu_1\gamma_s}, \tag{11}$$

$$P_f = \frac{k_o N}{2\omega\mu_2}\left(\frac{A_2^2}{2}d_1 + \frac{A_2^2}{4\gamma_f}\sin(2\gamma_f d_1) + \right. \\ \left. + \frac{A_3^2}{2}d_1 - \frac{A_3^2}{4\gamma_f}\sin(2\gamma_f d_1) + \frac{A_2 A_3}{\gamma_f}\sin^2(\gamma_f d_1)\right), \tag{12}$$

$$P_a = \frac{k_o N}{2\omega\mu_3}\left(\frac{A_4^2}{2\gamma_a}(e^{2\gamma_a d_2} - 1) - \right. \\ \left. - \frac{A_5^2}{2\gamma_a}(e^{-2\gamma_a d_2} - 1) + 2A_4 A_5 d_2\right), \tag{13}$$

$$P_c = \frac{k_o N A_6^2}{4\omega\mu_4\gamma_c}. \tag{14}$$

When the continuity requirement is applied to Eqs. (5)-(8) and their derivatives, the following relations between the constants A_1- A_6 are obtained,

$$A_1 = A_2, \tag{15}$$

$$A_2\cos(\gamma_f d_1) + A_3\sin(\gamma_f d_1) = A_4 + A_5, \tag{16}$$

$$A_4 e^{\gamma_a d_2} + A_5 e^{-\gamma_a d_2} = A_6, \tag{17}$$

$$A_1 = \frac{\gamma_f\mu_1}{\gamma_s\mu_2}A_3, \tag{18}$$

$$A_3\cos(\gamma_f d_1) - A_2\sin(\gamma_f d_1) = F \tag{19}$$

with

$$F = \frac{\gamma_a\mu_2}{\gamma_f\mu_3}(A_4 - A_5) \quad A_6 = \frac{\gamma_a\mu_4}{\gamma_c\mu_3}(A_5 e^{-\gamma_a d_2} - A_4 e^{\gamma_a d_2}). \tag{20}$$

2.3 Sensitivity of the Sensor

The sensitivity (S_{na}) of the evanescent field sensor is defined as the change of the effective refractive index with respect to the change of the adlayer refractive index n_a, i.e.,

$$S_{na} = \frac{\partial N}{\partial n_a}, \tag{21}$$

where $n_a = \sqrt{\varepsilon_3\mu_3}$.

Differentiating the dispersion relation given by Eq. (9) with respect to N, we get after a tedious derivation and mathematical manipulation

$$S_{na} = \frac{\{U_1(\sigma_{13} - \sigma_{19}) - U_2(\sigma_9 + \sigma_{19})\}}{\{(\sigma_1 - \sigma_2)(U_1^2 + U_2^2) + U_1(\sigma_{12} + \sigma_{18}) - U_2(\sigma_8 - \sigma_{18})\}}, \tag{22}$$

Where

$$U_1 = \gamma_a\mu_2(\gamma_a\mu_4 + \gamma_c) - (\gamma_a\mu_4 - \gamma_c)e^{-2\gamma_a d_2},$$

$$U_2 = \gamma_f(\gamma_a\mu_4 + \gamma_c) + (\gamma_a\mu_4 - \gamma_c)e^{-2\gamma_a d_2},$$

$$\sigma_1 = -\frac{k_o^2 N d_1}{\gamma_f},\ \sigma_2 = \frac{\gamma_f^2\mu_1\mu_2 k_o^2 N + \gamma_s^2\mu_1\mu_2 k_o^2 N}{\gamma_s\gamma_f(\gamma_f^2\mu_1^2 + \gamma_s^2\mu_2^2)},$$

$$\sigma_3 = \frac{k_o^2\mu_4 N}{\gamma_a},\ \sigma_4 = \frac{k_o^2\mu_4 n_a}{\gamma_a},\ \sigma_5 = \frac{k_o^2 N}{\gamma_c},$$

$$\sigma_6 = \frac{\mu_2 k_o^2 N(\gamma_a\mu_4 + \gamma_c)}{\gamma_a},\ \sigma_7 = \frac{\mu_2 k_o^2 n_a(\gamma_a\mu_4 + \gamma_c)}{\gamma_a},$$

$$\sigma_8 = \gamma_a\mu_2\sigma_3 + \gamma_a\mu_2\sigma_5 + \sigma_6,\ \sigma_9 = \gamma_a\mu_2\sigma_4 + \sigma_7,$$

$$\sigma_{10} = \frac{k_o^2\mu_4 N\gamma_a}{\gamma_f},\ \sigma_{11} = \frac{k_o^2 N\gamma_c}{\gamma_f},$$

$$\sigma_{12} = \gamma_f\sigma_3 + \gamma_f\sigma_5 - \sigma_{10} - \sigma_{11},\ \sigma_{13} = \gamma_f\sigma_4,$$

$$\sigma_{14} = \frac{-2d_2 k_o^2 N(\gamma_a\mu_4 - \gamma_c)}{\gamma_a},\ \sigma_{15} = \frac{2d_2 k_o^2 n_a(\gamma_a\mu_4 - \gamma_c)}{\gamma_a},$$

$$\sigma_{16} = \sigma_{14} + \sigma_3 - \sigma_5,\ \sigma_{17} = \sigma_{15} - \sigma_4,\ \sigma_{18} = \sigma_{16}e^{-2\gamma_a d_2},$$

$$\sigma_{19} = \sigma_{17}e^{-2\gamma_a d_2}.$$

The sensitivity (S_{d2}) of the effective index to any change in the adlayer thickness is calculated as the change of the effective index with respect to the change of the adlayer thickness d_2, i.e.,

$$S_{d2} = \frac{\partial N}{\partial d_2}, \tag{23}$$

$$S_{d2} = \frac{\rho_{13}(B_1 + B_2)}{\Phi_1 + \Phi_2 - (\rho_1 - \rho_2)(B_1^2 + B_2^2)}, \tag{24}$$

where

$$\rho_1 = -\frac{k_o^2 N d_1}{\gamma_f},\ \rho_2 = \frac{\gamma_f^2\mu_1\mu_2 k_o^2 N + \gamma_s^2\mu_1\mu_2 k_o^2 N}{\gamma_s\gamma_f(\gamma_f^2\mu_1^2 + \gamma_s^2\mu_2^2)},$$

$$\rho_3 = \frac{\mu_4 k_o^2 N}{\gamma_a},\ \rho_4 = \frac{k_o^2 N}{\gamma_c},\ \rho_5 = \gamma_a\mu_2\rho_3,\ \rho_6 = \gamma_a\mu_2\rho_4,$$

$$\rho_7 = \mu_2\mu_4 k_o^2 N,\ \rho_8 = \frac{\mu_2 k_o^2 N\gamma_c}{\gamma_a},\ \rho_9 = \gamma_f\rho_3,\ \rho_{10} = \gamma_f\rho_4,$$

$$\rho_{11} = \frac{\gamma_a\mu_4 k_o^2 N}{\gamma_f},\ \rho_{12} = \frac{\gamma_c k_o^2 N}{\gamma_f},\ \rho_{13} = -2e^{-2\gamma_a d_2}(\gamma_a^2\mu_4 - \gamma_a\gamma_c),$$

$$\rho_{14} = \frac{-2e^{-2\gamma_a d_2}(\gamma_a\mu_4 - \gamma_c)d_2 k_o^2 N}{\gamma_a},\ \rho_{15} = \rho_3 e^{-2\gamma_a d_2},$$

$$\rho_{16} = -\rho_4 e^{-2\gamma_a d_2},$$

$$B_1 = \gamma_a\mu_2(\gamma_a\mu_4 + \gamma_c) - (\gamma_a\mu_4 - \gamma_c)e^{-2\gamma_a d_2},$$

$$B_2 = \gamma_f(\gamma_a\mu_4 + \gamma_c) + (\gamma_a\mu_4 - \gamma_c)e^{-2\gamma_a d_2},$$

$$\Phi_1 = -\rho_9 B_1 - \rho_{10} B_1 + \rho_{11} B_1 + \rho_{12} B_1 - \rho_{14} B_1 - \rho_{15} B_1 - \rho_{16} B_1,$$

$$\Phi_2 = \rho_5 B_2 + \rho_6 B_2 + \rho_7 B_2 + \rho_8 B_2 - \rho_{14} B_2 - \rho_{15} B_2 - \rho_{16} B_2.$$

3. NUMERICAL RESULTS

Figure 1 shows the slab waveguide structure under consideration. In the numerical analysis we consider the operating wavelength of He-Ne laser ($\lambda = 632.8$ nm). The substrate is considered to be glass ($\varepsilon_1 = 2.16$ and $\mu_1 = 1$) covered by a LHM guiding layer with an electric permittivity ε_2 and magnetic permeability μ_2 of the forms $\varepsilon_2 = \varepsilon_{2r} + i\varepsilon_{2i}$ and $\mu_2 = \mu_{2r} + i\mu_{2i}$, respectively. The cladding is assumed to be water with index of refraction $n_3 = 1.33$. In order to optimize the sensitivity of the proposed sensor, it is significant to study the sensitivity dependence on different parameters of the LHM guiding film. In Fig. 2, the sensitivity (S_{na}) of the effective refractive index to any change in the adlayer index is displayed versus the guiding film thickness for different values of the real part of ε_2. As seen from the figure, the sensitivity has its maximum at LHM film thickness somewhat higher than cut-off thickness of the guided mode considered. At cut-off thickness, the sensitivity is almost zero since the effective refractive index is equal that of the substrate. For film thicknesses beyond the optimal value at which the sensitivity peaks, the sensitivity decreases to zero due to the large film thickness and high wave confinement. The behavior of S_{na} with the film thickness is exactly similar to that of three-layer conventional waveguide sensor which consists of three dielectric layers with the analyte is homogeneously distributed in the cladding layer [3, 29]. Decreasing the absolute value of the real part of ε_2 can noticeably improve the sensitivity without any observed effect on the optimal film thickness. For example, at $\varepsilon_2 = -3.2 + 0.01i$ the sensitivity has a maximum value 0.2823 whereas it has a maximum value of 0.3482 when $\varepsilon_2 = -2.8 + 0.01i$. This means a sensitivity improvement of 23.34 % can be reached when the real part of ε_2 changes from – 3.2 to – 2.8.

The effect of changing the imaginary part of the electric permittivity ε_2 on the sensitivity S_{na} is illustrated in Fig. 3. It is obvious that changing the imaginary part of ε_2 in the range from 0.01 to 0.05 has barely detectable effect on the sensitivity of the effective refractive index to any change in the adlayer index.

Figure 4 shows the sensitivity of the proposed sensor as a function of the LHM film thickness for different real parts of magnetic permeability μ_2 of the LHM. The real parts of ε_2 and μ_2 have almost the same effect on the sensitivity. The sensitivity can be enhanced with decreasing the absolute value of the real part of any of them. The most important feature that can be seen is the optimal thickness at which the sensitivity peaks does not depend on the real parts of ε_2 and μ_2. As Fig. 4 shows, when $\mu_2 = -5.2 + 0.01i$ the sensitivity has a maximum value of 0.2486 whereas it has a maximum

value of 0.3805 when $\mu_2 = -4.8 + 0.01i$. A sensitivity enhancement of 53.06 % can be obtained when the real part of μ_2 changes from -5.2 to -4.8. The effect of the real part of μ_2 on the sensitivity is much higher than that of the real part of ε_2. Changing the imaginary part of μ_2 has much less effect on the sensitivity than the real part as shown in Fig. 5. When the imaginary part of μ_2 changes from 0.01 to 0.05, the maximum sensitivity decreases from 0.3159 to 0.2844. Comparing Figs. 2 and 4, and Figs. 3 and 5, it is clear that the electric permittivity ε_2 has much less effects on the sensitivity than the magnetic permeability μ_2. This may be attributed to the TE modes considered in this work in which the dispersion relation appears in terms of μ.

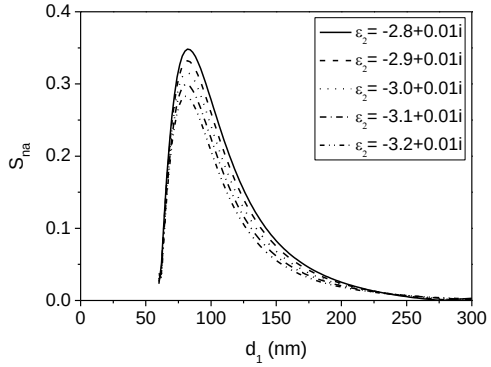

Fig. 2 – S_{na} versus the guiding film thickness for different real parts of ε_2 for $d_3 = 20$ nm, $\varepsilon_1 = 2.16$, $\varepsilon_3 = 2.37$, $\varepsilon_4 = 1.77$, $\mu_1 = 1$, $\mu_2 = -0.5 + 0.01i$, $\mu_3 = 1$, and $\mu_4 = 1$

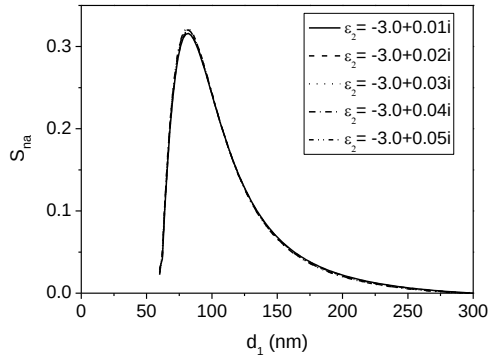

Fig. 3 – S_{na} versus the guiding film thickness for different imaginary parts of ε_2 for $d_3 = 20$ nm, $\varepsilon_1 = 2.16$, $\varepsilon_3 = 2.37$, $\varepsilon_4 = 1.77$, $\mu_1 = 1$, $\mu_2 = -0.5 + 0.01i$, $\mu_3 = 1$, and $\mu_4 = 1$

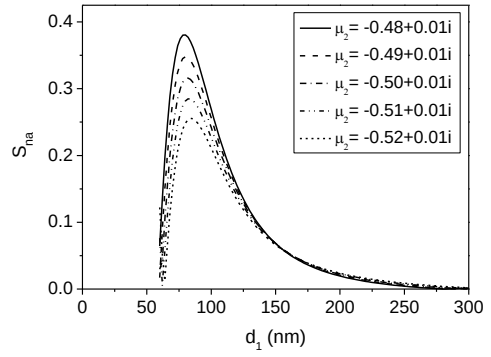

Fig. 4 – S_{na} versus the guiding film thickness for different real parts of μ_2 for $d_3 = 20$ nm, $\varepsilon_1 = 2.16$, $\varepsilon_2 = -3 + 0.01i$, $\varepsilon_3 = 2.37$, $\varepsilon_4 = 1.77$, $\mu_1 = 1$, $\mu_3 = 1$, and $\mu_4 = 1$

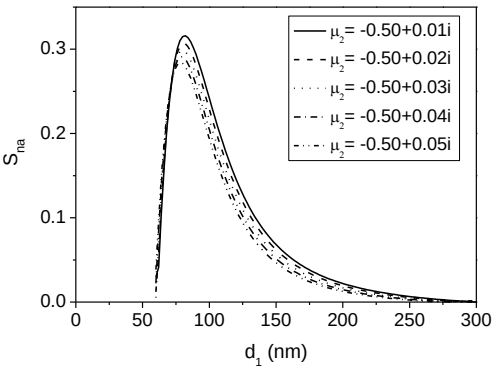

Fig. 5 – S_{na} versus the guiding film thickness for different imaginary parts of μ_2 for $d_3 = 20$ nm, $\varepsilon_1 = 2.16$, $\varepsilon_2 = -3 + 0.01i$, $\varepsilon_3 = 2.37$, $\varepsilon_4 = 1.77$, $\mu_1 = 1$, $\mu_3 = 1$, and $\mu_4 = 1$

We now turn our attention to investigating the sensitivity (S_{d2}) of the effective refractive index of the guided mode to any change in the adlayer thickness. In Fig. 6, the effect of the real part of ε_2 on the sensitivity of the proposed sensor to the change in the adlayer thickness is illustrated. In general, the proposed sensor exhibits a low sensitivity of order 10^{-4} to the adlayer thickness change. The real part of ε_2 plays a significant role in the enhancement of S_{d2}. The peak value of S_{d2} increases from 5.686×10^{-4} to 7.732×10^{-4} as the real part of ε_2 changes from -3.2 to -2.8. This indicates a sensitivity improvement of 35.98 %. The sensitivity does not exhibit a considerable dependence on the imaginary part of ε_2 as shown in Fig. 7. Figures 8 and 9 show S_{d2} versus the LHM layer thickness for different values of the real and imaginary parts of μ_2, respectively. As can be seen from Fig. 8, when $\mu_2 = -5.2 + 0.01i$ the sensitivity has a maximum value of 5.360×10^{-4} whereas it has a maximum value of 8.267×10^{-4} when $\mu_2 = -4.8 + 0.01i$. A sensitivity enhancement of 54.18 % can be obtained. We again notice that the effect of the real part of μ_2 on S_{d2} is much higher than that of the real part of ε_2.

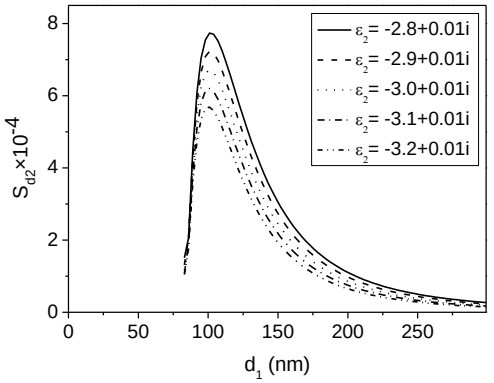

Fig. 6 – S_{d2} versus the guiding film thickness for different values of the real part of ε_2 for $d_3 = 20$ nm, $\varepsilon_1 = 2.16$, $\varepsilon_3 = 2.37$, $\varepsilon_4 = 1.77$, $\mu_1 = 1$, $\mu_2 = -0.5 + 0.01i$, $\mu_3 = 1$, and $\mu_4 = 1$

It is significant to study the performance of the proposed sensor for different adlyers. In Figs. 10 and 11, we investigate the behavior of the sensitivities versus the LHM thickness for different proteins solved in the same concentration of the solvent (0.1 N KOH) which are Globin and Gliadin with refractive indices $n_a = 1.535$

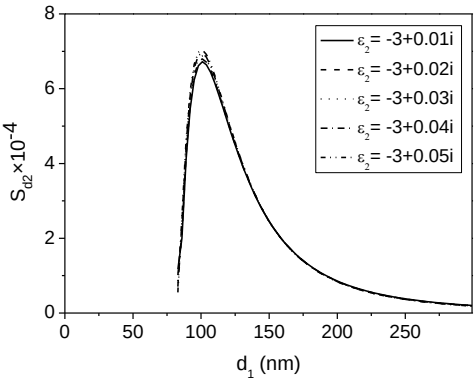

Fig. 7 – S_{d2} versus the guiding film thickness for different imaginary parts of ε_2 for $d_3 = 20$ nm, $\varepsilon_1 = 2.16$, $\varepsilon_3 = 2.37$, $\varepsilon_4 = 1.77$, $\mu_1 = 1$, $\mu_2 = -0.5 + 0.01i$, $\mu_3 = 1$, and $\mu_4 = 1$

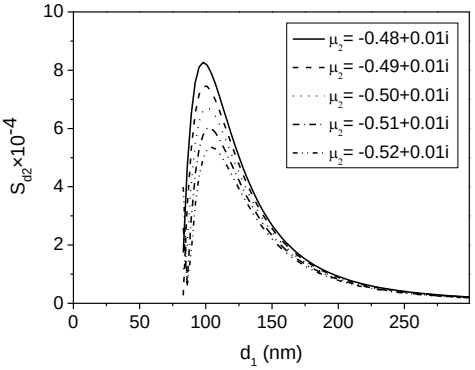

Fig. 8 – S_{d2} versus the guiding film thickness for different real parts of μ_2 for $d_3 = 20$ nm, $\varepsilon_1 = 2.16$, $\varepsilon_2 = -3 + 0.01i$, $\varepsilon_3 = 2.37$, $\varepsilon_4 = 1.77$, $\mu_1 = 1$, $\mu_3 = 1$, and $\mu_4 = 1$

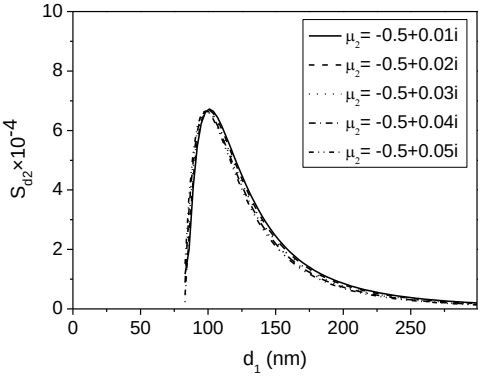

Fig. 9 – S_{d2} versus the guiding film thickness for different imaginary parts of μ_2 for $d_3 = 20$ nm, $\varepsilon_1 = 2.16$, $\varepsilon_2 = -3 + 0.01i$, $\varepsilon_3 = 2.37$, $\varepsilon_4 = 1.77$, $\mu_1 = 1$, $\mu_3 = 1$, and $\mu_4 = 1$

and $n_a = 1.556$, respectively [30]. As seen from Fig. 10, S_{na} peaks at an optimal LHM thickness of 83 nm and reaches a maximum value of 0.315 for Globin adlyer. On the hand, it reaches a maximum value of 0.283 at an optimal thickness of 80 nm for Gliadin adlayer. Figure 11 shows that S_{d2} can reach a maximum value of 6.721×10^{-4} at an optimal thickness of 101 nm for Globin adlyer whereas it reaches a maximum value of 7.008×10^{-4} at an optimal thickness of 98 nm for Gliadin adlayer. Therefore, we may conclude that each protein adlayer has its own maximum sensitivity and optimal thickness. Thus each protein is characterized by its sensitivity curve which can be used as an ID code for it.

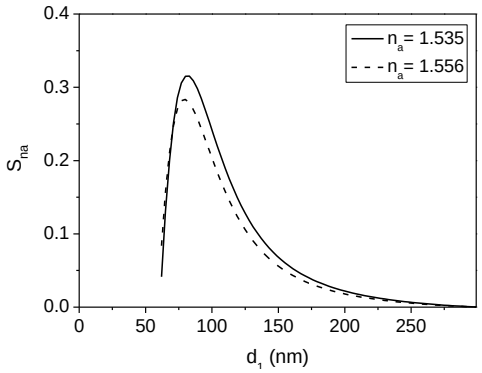

Fig. 10 – S_{na} versus the guiding film thickness for different n_a for $d_3 = 20$ nm, $\varepsilon_1 = 2.16$, $\varepsilon_2 = -3 + 0.01i$, $\varepsilon_4 = 1.77$, $\mu_1 = 1$, $\mu_2 = -0.5 + 0.01i$, $\mu_3 = 1$, and $\mu_4 = 1$

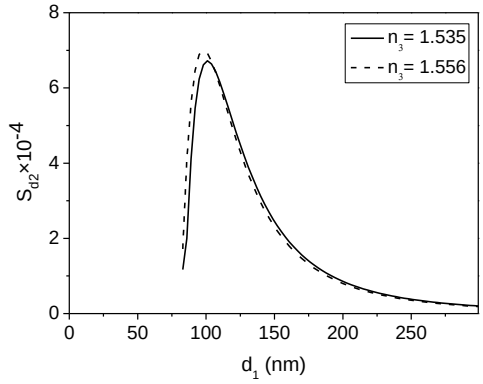

Fig. 11 – S_{d2} versus the guiding film thickness for different n_a for $d_3 = 20$ nm, $\varepsilon_1 = 2.16$, $\varepsilon_2 = -3 + 0.01i$, $\varepsilon_4 = 1.77$, $\mu_1 = 1$, $\mu_2 = -0.5 + 0.01i$, $\mu_3 = 1$, and $\mu_4 = 1$

4. CONCLUSION

We considered a four-layer waveguide structure as an optical sensor for detection any change in an adlayer thickness and refractive index. The guiding film was assumed to be a lossy left-handed material. The sensitivities of the effective refractive index of the guided mode to any change in the refractive index/thickness of the adlayer were derived and investigated. We found a set of significant features. First, a slight change in the real parts of the permittivity and permeability of the LHM can significantly improve the sensitivity of the proposed sensor. Second, the imaginary parts of the permittivity and permeability of the LHM have barely detectable effects on the sensitivity of the proposed sensor. Third, the electric permittivity of the LHM has much less effects on the sensitivity than the magnetic permeability. Forth, each protein adlayer has its own maximum sensitivity and optimal thickness. Thus each protein is characterized by its sensitivity curve which can be used as an ID code for it.

ACKNOWLEDGEMENT

The authors would like to express gratitude to the ministry of higher education (scientific research council) for the financial support of this work.

REFERENCES

1. S.A. Taya, T.M. El-Agez, *Turk. J. Phys.* **35** No 1, 31 (2011).
2. O. Parriaux, G. Velduis, *J. Lightwave Technol.* **16** No 4, 573 (1998).
3. T.M. El-Agez, S.A. Taya, *Opt. Applicata* **41** No 1, 89 (2011).
4. N. Skivesen, R. Horvath, H. Pedersen, *Opt. Lett.* **30** No 13, 1659 (2005).
5. S.A. Taya, T.M. El-Agez, *J. Opt.* **13** No 7, 075701 (2011).
6. M. Zourob, S. Mohr, P.R. Fielden, N.J. Goddard, *Sensor. Actuat. B* **94** No 3, 304 (2003).
7. S.A. Taya, E.J. El-Farram, T.M. El-Agez, *Int. J. Electron. Commun. (AEÜ)* **66** No 3, 204 (2012).
8. S.A. Taya, T.M. El-Agez, *Turk. J. Phys.* **36** No 1, 67 (2012).
9. G. Tollin, Z. Salamon, *Biophys. J.* **80** No 3, 1557 (2001).
10. S.A. Taya, T.M. El-Agez, *Optik* **123** No 5, 417 (2012).
11. H.M. Kullab, S.A. Taya, T.M. El-Agez, *J. Opt. Soc. Am. B* **29** No 5, 959 (2012).
12. H.M. Kullab, S.A. Taya, *Int. J. Electron. Commun. (AEÜ)* **67** No 11, 905 (2013).
13. H.M. Kullab, S.A. Taya, *Optik* **125** No 1, 97 (2014).
14. S.A. Taya, H.M. Kullab, *Appl. Phys. A* **116** No 4, 1841 (2014).
15. S.A. Taya, *Opto-Electron. Rev.* **22** No 4, 252 (2014).
16. V. Veselago, *Sov. Phys. Usp.* **10** No 4, 509 (1968).
17. K. Park, B.J. Lee, C. Fu, Z.M. Zhang, *J. Opt. Soc. Am. B* **22** No 5, 1016 (2005).
18. S.A. Taya, E.J. El-Farram, M.M. Abadla, *Optik* **123** No 24, 2264 (2012).
19. S.A. Taya, I.M. Qadoura, *Optik* **124** No 13, 1431 (2013).
20. A. Alu, N. Engheta, *Phys. Rev. E* **72** No 1, 016623 (2005).
21. J.B. Pendry, *Phys. Rev. Lett.* **85** No 18, 3966 (2000).
22. I.M. Qadoura, S.A. Taya, K.Y. El-wasife, *Int. J. Microwave Opt. Technol. (IJMOT)* **7** No 5, 349 (2012).
23. S.A. Taya, H.M. Kullab, I.M. Qadoura, *J. Opt. Soc. Am. B* **30** No 7, 2008 (2013).
24. N. Fang, H. Lee, C. Sun, X. Zhang, *Science* **308** No 5721, 534 (2005).
25. S.A. Taya, K.Y. Elwasife, H.M. Kullab, *Opt. Applicata* **43** No 4, 857 (2013).
26. M. Abadla, S.A. Taya, *Optik* **125** No 3, 1401 (2014).
27. Q. Bai, J. Chen, N. Shen, C. Cheng, H. Wang, *Opt. Express* **18** No 3, 2106 (2012).
28. S.A. Taya, K.Y. Elwasife, *J. Nano- Electron. Phys.* **6** No 2, 02007 (2014).
29. K. Tiefenthaler, W. Lukosz, *J. Opt. Soc. Am. B* **6** No 2, 209 (1989).
30. D.B. Hand, *J. Biol. Chem.* **108** No 3, 703 (1935).
31. S.A. Taya, *J. Magn. Magn. Mater.* **377**, 281 (2015).